The Journal of Experimental Biology 210, 2593-2606
Published by The Company of Biologists 2007
doi:10.1242/jeb.002071

Aerodynamic force generation, performance and control of body orientation during gliding in sugar gliders (*Petaurus breviceps*)

Kristin L. Bishop

Department of Ecology and Evolutionary Biology, Brown University, Providence, RI 02912, USA

Present address: Section of Ecology and Evolution, University of California, Davis, Davis, CA 95616, USA (e-mail: kvwbishop@ucdavis.edu)

Accepted 24 March 2007

Summary

Gliding has often been discussed in the literature as a possible precursor to powered flight in vertebrates, but few studies exist on the mechanics of gliding in living animals. In this study I analyzed the 3D kinematics of sugar gliders (*Petaurus breviceps*) during short glides in an enclosed space. Short segments of the glide were captured on video, and the positions of marked anatomical landmarks were used to compute linear distances and angles, as well as whole body velocities and accelerations. From the whole body accelerations I estimated the aerodynamic forces generated by the animals. I computed the correlations between movements of the limbs and body rotations to examine the control of orientation during flight. Finally, I compared these results to those of my earlier study on the similarly sized and distantly related southern flying squirrel (*Glaucomys volans*).

The sugar gliders in this study accelerated downward slightly ($1.0\pm0.5\ m\ s^{-2}$), and also accelerated forward ($2.1\pm0.6\ m\ s^{-2}$) in all but one trial, indicating that the body weight was not fully supported by aerodynamic forces and that some of the lift produced forward acceleration rather than just balancing body weight. The gliders used high angles of attack ($44.15\pm3.12^{\circ}$), far higher than the angles at which airplane wings would stall, yet generated higher lift coefficients (1.48 ± 0.18) than would be expected for a stalled wing. Movements of the limbs were strongly correlated with body rotations, suggesting that sugar gliders make extensive use of limb movements to control their orientation during gliding flight. In addition, among individuals, different limb movements were associated with a given body rotation, suggesting that individual variation exists in the control of body rotations. Under similar conditions, flying squirrels generated higher lift coefficients and lower drag coefficients than sugar gliders, yet had only marginally shallower glides. Flying squirrels have a number of morphological specializations not shared by sugar gliders that may help to explain their greater lift generating performance.

Supplementary material available online at
http://jeb.biologists.org/cgi/content/full/210/15/2593/DC1

Key words: aerodynamics, biomechanics, gliding, mammal, stability.

Introduction

Although gliding is the simplest form of flight, surprisingly little is known about the mechanics of gliding in animals. Some vertebrate gliders do not possess anything that we would recognize as wings (Emerson and Koehl, 1990; McCay, 2001a; Socha, 2002), and in those that do, the wings differ from human engineered wings in shape, material composition and typical flight speeds, so standard aerodynamic theory may not accurately predict animal gliding performance (Bishop, 2006; McGuire and Dudley, 2005; Socha et al., 2005). Form and function are related to evolutionary fitness through the performance of tasks that are critical to survival and reproduction, such as locomotion. An understanding of the mechanistic basis for differences in performance provides valuable groundwork upon which to base studies of the evolutionary history and diversity of organisms.

In addition to being interesting as a form of locomotion in its own right, mammalian gliding is of particular interest due to its probable role in the evolution of flapping flight in bats. It is widely believed that bats evolved from an arboreal gliding ancestor similar to extant gliding mammals (Clark, 1978; Smith, 1976; Norberg, 1985; Norberg, 1990; Simmons, 1995; Bishop, 2006). The transition from gliding to flapping flight presents an interesting evolutionary problem. Gliding and flapping flight are very different behaviors and may be subject to different optimization criteria (Padian, 1982). Mammalian glider wings differ consistently from bat wings in being very short spanwise relative to their breadth, i.e. having a very low aspect ratio (AR), and in being nearly rectangular in shape compared to the tapering wings of bats. Experiments with physical models of wings have shown that wings with AR<2, as possessed by all mammalian gliders, have very different aerodynamic properties than wings with AR>2, as are typical of bats, such that aerodynamic performance declines with increasing AR in the low AR range and improves with increasing AR in the high AR range (Torres and Mueller, 2001; Shyy et al., 2005; Galvao et

al., 2006). How is it possible to move between two such highly specialized states without going through a phase in which the animal is not particularly well adapted for either function?

Previous studies have modeled an evolutionary transition from gliding to flapping flight by assuming that flapping evolved to extend the flight distance (Bock, 1965; Parkes, 1966; Norberg, 1985). Flight distance is extended by altering the production of aerodynamic forces. The measure of performance most commonly used is the glide ratio (Vernes, 2001; Stafford et al., 2002; Jackson, 2000), the horizontal distance traveled divided by the vertical drop, because it is a measure of the distance an animal can travel from a given height. In a steady, non-accelerating glide, the glide ratio is determined by the ratio of lift to drag, the aerodynamic forces perpendicular to the direction of travel and parallel and opposite to the direction of travel, respectively. The lift-to-drag ratio can be increased by increasing lift, decreasing drag, and/or by producing thrust, defined as a force that opposes drag. Flapping has often been assumed to have evolved as a means to increase lift and thrust (Bock, 1965; Parkes, 1966; Norberg, 1985), thereby increasing the distance traveled, but other potentially important features of flight performance have typically been overlooked.

Although producing lift and thrust is certainly important to powered fliers, controlling the flight trajectory is equally important, and the roles of stability and maneuverability have often been overlooked in discussions of gliding performance. It has been suggested that flapping movements of wings such as those possessed by mammalian gliders would cause rotational instabilities that could lead to problems with control (Caple et al., 1983). It is possible, however, that gliding animals actively employ movements of the limbs to counter rotational motions during a glide (Bishop, 2006), and further, that the earliest flapping behavior may have been used for stability and maneuverability and not simply for lift or thrust. Specialized gliding frogs have been found to be passively unstable gliders (McCay, 2001b), suggesting that they must actively control their glide using body movements. An understanding of how gliding flight is actively controlled by limb movements is critical to developing viable models of a gliding to flapping transition.

In this study, I examined gliding in a specialized mammalian glider, the marsupial sugar glider *Petaurus breviceps* (Waterhouse) using video images captured using two high-speed video cameras to reconstruct the 3D coordinates of anatomical landmarks. I investigated the relationships among details of gliding kinematics, aerodynamic force generation, and gliding performance, with special attention to assessing control of the glide trajectory by documenting the relationship between limb movements and body rotations. Finally, I compared gliding in *P. breviceps* to that in a placental gliding specialist, *Glaucomys volans*, the southern flying squirrel. Relationships between kinematics and performance that are similar in diverse groups of mammals may have also governed gliding in bat ancestors and provide a basis for hypotheses about the origin of flapping in bats. This study represents the first interspecific comparison of the detailed 3D kinematics of gliding in mammals and is the first to document the role of limb movements in controlling body rotations in any glider.

Materials and methods

I used high-speed video of marsupial sugar gliders *Petaurus breviceps* (Waterhouse) during short glides in a controlled, laboratory setting to reconstruct detailed, 3D kinematics of the glide. These data allowed me to document the animals' body positions, estimate the aerodynamic forces they generated, and measure glide angle, velocity and body rotations, all of which are potentially ecologically relevant performance features.

Data collection

Four sugar gliders were purchased at weaning through the pet trade and maintained in the animal care facility at Brown University in accordance with institutional animal care procedures (IACUC #16-06). The animals were housed in a large cage with ample room to run and jump, and food and water were provided *ad libitum*. After a 1-week period of hand taming, the animals were trained on a daily basis to jump, then glide to a PVC pole with a diameter similar to that of a large tree trunk. Training continued until adult size had been reached (approximately 4 months old), at which time filming commenced. At the time of filming, the mean body length of the animals was 13.5 cm from the tip of the nose to the base of the tail and their mean body mass was 73.4 g. During the training period, the gliders were given food rewards to promote gliding behavior, but no food rewards were given during filming to ensure the accuracy of weight measurements taken just before data collection.

Filming took place in a large garage with a high ceiling at Harvard University's Concord Field Station using a pair of high-speed digital video cameras (Redlake, PCI-1000, San Diego, CA, USA) at a framing rate of 250 Hz and an image size of 480×420 pixels. The cameras were placed beneath the glide path at an angle of approximately 90° to one another (Fig. 1). The volume of space visible in both cameras was calibrated in three dimensions using a 0.57 m×0.49 m×0.41 m pre-measured calibration frame (Peak Performance, Inc., Englewood, CO, USA). The cameras were positioned such that

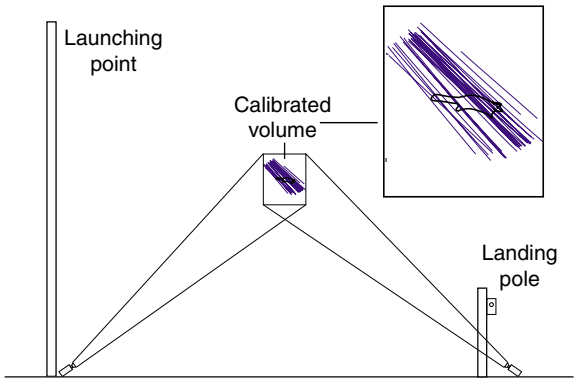

Fig. 1. Experimental set-up, drawn to scale. Sugar gliders were trained to glide from a launching pole to a landing pole in an enclosed space. Two high-speed digital cameras were positioned beneath the glide path at approximately 90° to one another. The calibrated volume of space visible in both cameras is represented by the box surrounding the glider. The blue lines are computed trajectories of the sternum through the space for all glide sequences.

the calibration frame occupied as much of the field of view as possible in both cameras so that when the animal was visible in both cameras, it was also in the calibrated volume, with some exception at the edges of the field of view. Consequently, the volume of the overlapping fields of view of the cameras was approximately equal to the volume of the calibration object.

Using medical adhesive [Silastic(R) type A, Dow Corning, Midland, MI, USA], 6 mm diameter spherical reflective markers were attached to the skin at the sternum, pubic symphysis (hereafter called the pelvis marker), right and left hip joint, left wrist, left ankle and the center of the free edge of the left patagium (Fig. 2). The markers were placed ventrally so that they could be seen from the cameras beneath the glide path. Because an additional point on the body axis was needed for some of the analyses, the nose was also treated as a landmark.

The gliders launched from a height of approximately 4 m from a 5 cm diameter PVC pipe to a 10 cm diameter vertical landing pole placed at a horizontal distance of approximately 4 m from the launching site (Fig. 1). The launching pole was covered with window screening to provide traction and the landing pole was covered with carpet padding to provide a soft landing. 55 glides were analyzed; of these, six were excluded from body rotation analysis because the right hip marker had fallen off. The length of the video sequences ranged from 0.12–0.19 s (30–48 frames).

Video sequences were digitized using DLT DataViewer 2 (http://faculty.washington.edu/thedrick/digitizing/) in Matlab (MathWorks, Natick, MA, USA). I estimated digitizing error by digitizing the same trial five times and computing the standard deviation for the five trials for each point in each frame, then taking the mean of the standard deviations of all the frames for each point. This mean of the standard deviations is henceforth referred to as the digitizing error. The digitizing error was approximately 1 mm in each dimension for points with a visible marker and 3 mm for points that were visually estimated.

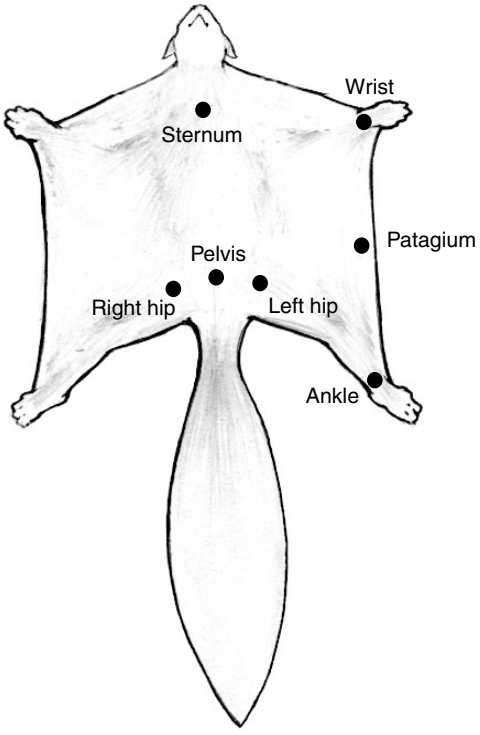

Fig. 2. Placement of reflective body markers. The chord line is the line connecting the wrist and ankle markers. The 'mean hip' is the mean of the positions of the right and left hip.

Random digitizing error can have a disproportionate effect on computed quantities. To estimate this effect, I simulated random noise by adding or subtracting a random number up to the estimated digitizing error to each coordinate (x,y,z) for a representative trial. I then calculated resulting distances, velocities, accelerations and angles for the data with simulated error. This was repeated 10 000 times; digitizing error for the computed quantities was estimated as the standard deviation of the replicate computations. For linear measurements the digitizing errors were all less than 0.5 mm, a maximum of a 2% error. For velocity measurements, the standard deviations were less than 0.002 m s^{-1}, representing a 0.04% error. Accelerations had standard deviations of less than 0.01 m s^{-2} and errors of less than 5%. Angular measurements were accurate to 0.5° with errors of less than 3%, with the exception of roll angle, which had errors of nearly 6%. The residuals of direct linear transformations, which incorporate both the spatial error of the calibration and digitizing error, were approximately 1 mm for all points in all dimensions.

Performance measures

An animal may glide for many reasons, such as to reach distant food resources, escape predators, or return to nest sites. Because the relevant aspect of performance depends on the specific task being performed, no single measure of performance is sufficient to characterize overall gliding performance. Therefore, in this study I consider three aspects of performance that appear to be particularly important: glide angle, glide velocity and stability. All of these performance parameters depend on the animal's manipulation of the aerodynamic forces it generates.

The position data were smoothed using a curve-fit method to compute whole body velocity and acceleration. A second-degree polynomial was fit to the position data for the sternum and pelvis markers and the polynomials were differentiated twice to compute the velocity and acceleration, respectively. The second-degree polynomials provided a good fit to the data, with maximum residual errors of 0.6%, indicating that acceleration was essentially constant in all directions over these short glide segments.

The position of the center of mass was estimated using a cadaver specimen that was frozen in a position similar to that adopted in flight, and was found to lie near the midpoint between where the sternum and hip marker were placed. Because the center of mass is approximately mid-way between the sternum and the hip, and assuming minimal spinal flexion, whole-body velocities and accelerations were estimated as the averages of those of these two landmarks. To the extent that the center of mass deviates from this position, a small error will be introduced into the estimates by any body rotations about the center of mass.

Glide angle is defined as the angle between the animal's glide trajectory and the horizontal (Fig. 3). More shallow glides have lower glide angles, while steeper glides have higher glide

angles. In a steady, non-accelerating glide, the glide angle is inversely proportional to the lift-to-drag ratio (Fig. 3A), so horizontal distance traveled from a given height is maximized by generating a large amount of lift relative to drag. Glide angle was computed for each frame as:

$$\theta = \arctan(V_y/V_x)\,, \quad (1)$$

where θ is the glide angle, V_y is the vertical component of the whole body velocity, and V_x is the forward component of the whole body velocity.

Forces

Drag and lift, the aerodynamic forces parallel and opposite, and perpendicular to the direction of travel, respectively, were estimated from the whole body accelerations. In a steady, non-accelerating glide, the resultant aerodynamic force is equal to and opposite the body weight, Mg, where M is mass and g is acceleration due to gravity (Fig. 3A). The animals in this study, however, accelerated both horizontally forward and vertically downward, necessitating a more complicated force balance to estimate the aerodynamic forces (Fig. 3B).

A positive horizontal acceleration indicates that the resultant aerodynamic force is inclined forward with respect to the vertical. The forward component of the resultant force was computed as the animal's body mass × the forward component of its acceleration. The two forces acting vertically on a gliding animal are its body weight and the vertical component of the resultant aerodynamic force (Fig. 3B). In a non-accelerating glide the vertical resultant aerodynamic force is equal to body mass × acceleration due to gravity. However, the net downward acceleration in these glides indicates that the entire body weight was not balanced by the vertical component of the resultant aerodynamic force. Therefore, I computed the vertical component of the resultant aerodynamic force by subtracting the measured vertical acceleration from the acceleration due to gravity before multiplying by the body mass.

Because drag is defined as a force acting parallel and opposite to the direction of the whole-body velocity, I used the angle between the opposite of the velocity vector and the resultant aerodynamic force vector to decompose the resultant aerodynamic force into lift and drag components (Fig. 3B). The reference angle between drag and the resultant aerodynamic force is:

$$\varphi = \arccos\frac{-\mathbf{V}\bullet\mathbf{R}}{|-\mathbf{V}|\times|\mathbf{R}|}\,, \quad (2)$$

where $-\mathbf{V}$ is the opposite of the velocity vector and $\mathbf{R}$ is the aerodynamic force vector. Lift and drag were then computed as:

$$L = R\sin\varphi;\ D = R\cos\varphi\,, \quad (3)$$

where L is lift, D is drag, R is the magnitude of the resultant aerodynamic force, and φ is the reference angle between drag

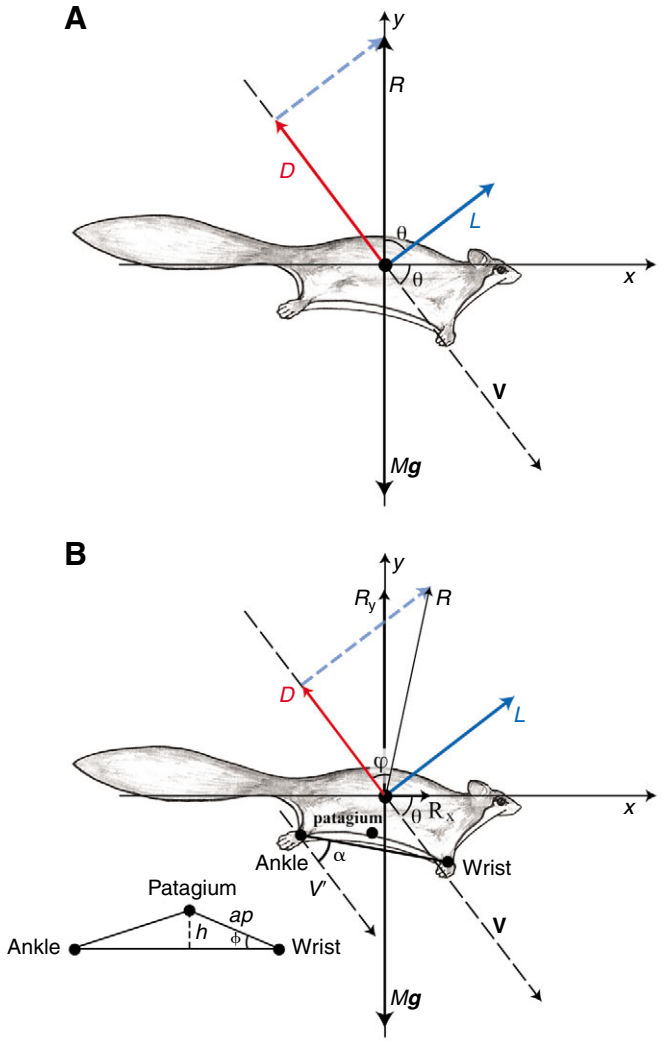

Fig. 3. Force balance diagrams for gliding and computation of angle of attack and camber. (A) Steady (non-accelerating) glides. The resultant aerodynamic force is oriented vertically and is equal to mass × acceleration due to gravity. The angle between the resultant aerodynamic force vector and the lift vector is equal to the glide angle, so lift and drag can be computed as the magnitude of the resultant aerodynamic force × the cosine and sine, respectively, of the glide angle. The lift-to-drag ratio is equal to the cotangent of the glide angle, and is therefore inversely proportional to it. (B) Non-steady (accelerating) glides. Horizontal accelerations indicate that the resultant aerodynamic force is inclined with respect to the vertical and vertical accelerations indicate that the magnitude of the vertical component of the resultant aerodynamic force is not equal to mass times acceleration due to gravity. More complicated computations of lift and drag are required (see text) and there is no necessary relationship between lift-to-drag ratio and glide angle. Angle of attack is the angle between a line connecting the wrist and ankle and the direction of the whole body velocity. See text for details on calculations. Camber is computed as the perpendicular distance from the patagium marker to a line connecting the wrist and ankle. The 3D angle between the chord line and the line connecting the wrist and the patagium marker is computed as a reference. Camber height is estimated as the distance from the wrist to the patagium marker times the sine of the reference angle. **V,** velocity vector; V', direction of velocity vector; R, resultant aerodynamic force vector; M, mass of glider; g, acceleration due to gravity; L, lift; D, drag; θ, glide angle; φ, reference angle between drag and the resultant aerodynamic force; α, angle of attack; h, camber height; ap, anterior patagium distance (between wrist and patagium markers); ϕ, reference angle between chord line and anterior patagium line.

and the resultant aerodynamic force. To compare airfoils of different sizes operating at different speeds, these forces are typically converted into dimensionless force coefficients:

$$C_{\mathrm{L}} = \frac{2L}{\rho V^2 S} = \frac{2R\sin\varphi}{\rho V^2 S}; \quad C_{\mathrm{D}} = \frac{2D}{\rho V^2 S} = \frac{2R\cos\varphi}{\rho V^2 S}, \qquad (4)$$

where C_{L} and C_{D} are the lift and drag coefficients, V is velocity and S is the wing area. These coefficients serve to quantify the effect on force generation of factors such as shape, orientation of the wing in space, and surface properties of the wing, which cannot be predicted quantitatively.

Body rotations

The three rotational axes are pitch, roll and yaw. The rotational angles of the body were computed sequentially in the order: yaw, pitch, roll. Rotating the coordinate system in this order results in an animal-centered coordinate system with the frontal plane of the body as the *x*–*z* (horizontal) plane. The coordinates for all of the points were recalculated after each rotation, and the next rotation was computed based on the new coordinates, resulting in an animal-centered coordinate system with the horizontal plane defined by the sternum, right hip and left hip of the animal and with the sternum at the origin. This plane will henceforth be referred to as the body plane. For the purposes of this discussion I use capital letters to refer to global coordinates and lower case letters to refer to animal-centered coordinates.

Yaw is defined as a rotation about the *Y* (vertical) axis. I defined the body axis by taking the mean of the left and right hip coordinates (hereafter called 'mean hip') and computing the coordinates of the sternum with respect to that point. I define the yaw angle as the angle between a line joining the sternum and mean hip and the *X* (forward) axis, computed as:

$$\mathrm{Yaw} = \arctan(Z_{\mathrm{ste}}/X_{\mathrm{ste}}), \qquad (5)$$

where Z_{ste} and X_{ste} are the lateral and fore–aft coordinates of the sternum with respect to the mean of the hip coordinates. A positive yaw angle occurs when the sternum is to the right of the mean hip and negative when it is to the left. All coordinates were then rotated by the yaw angle for each frame before computing the pitch angle.

Pitch is defined as a rotation about the mediolateral axis and was computed as the angle between a line connecting the sternum and mean of the hip coordinates and the yaw-corrected *x* axis:

$$\mathrm{Pitch} = \arctan(Y_{\mathrm{ste}}/x_{\mathrm{ste}}), \qquad (6)$$

where Y_{ste} and x_{ste} are the yaw-corrected *x* and *Y* positions of the sternum relative to the mean hip coordinates. Pitch is positive when the sternum is higher than the hips (nose-up rotation) and negative when it is lower (nose-down). All coordinates were then rotated by the pitch angle in each frame of the video sequence.

Roll is defined as rotation about the anteroposterior axis. It is computed as the angle between a line connecting the right and left hip and the yaw and pitch-corrected *z* (lateral) axis:

$$\mathrm{Roll} = \arctan(y_{\mathrm{rhip}}/z_{\mathrm{rhip}}), \qquad (7)$$

where y_{rhip} and z_{rhip} are the yaw and pitch-corrected positions of the right hip with respect to the left hip. Roll is positive when the right hip is higher than the left hip and negative when it is lower. The coordinate system was then rotated by the roll angle in each frame such that the *x*–*z* plane is equal to the plane formed by the sternum and right and left hips.

Limb positions

The angle of attack of a wing is defined as the angle between the chord line, a line joining the leading and trailing edges of the wing, and the direction of the oncoming airflow. In the case of a gliding animal, the direction of the oncoming airflow is determined by the glide angle. The angle of attack is important aerodynamically because within a range of low angles of attack, lift increases with increasing angle of attack. Beyond this range, as the angle of attack gets larger, the airflow begins to separate from the surface of the wing and the wing begins to stall. At angles of attack beyond the stall angle, lift decreases with increasing angle of attack. Because more of the wing's surface is exposed to the air flow as angle of attack increases, drag increases with increasing angles of attack up to 90°.

Angle of attack was computed for each frame as the angle between the chord line, a line connecting the wrist and ankle, and the velocity vector (Fig. 3B) using the following equation:

$$\alpha = \arccos\frac{\mathbf{V}\bullet\mathbf{C}}{|\mathbf{V}|\times|\mathbf{C}|}, \qquad (8)$$

where **V** is the velocity vector and **C** is the chord vector formed by placing the ankle at the origin and pointing to the wrist. Because only the chordwise component of flow over the wing matters to the effect of angle of attack, this angle was computed as a 2D angle in the parasagittal (*X*–*Y*) plane.

The camber of a wing is defined as its curvature from leading edge to trailing edge. A gliding mammal can theoretically control the camber of its wings in one or both of two ways. It can move its fore- and hindlimbs closer to one another, increasing the slackness of the wing membrane and allowing more billowing. Gliding mammals also have musculature within the wing membrane (Johnson-Murray, 1977; Johnson-Murray, 1987; Endo et al., 1998). Although the function of these muscles has not been tested, they are positioned such that if contracted or relaxed they may allow lesser or greater billowing of the wing.

The amount of lift a wing can generate increases with increasing camber up to the point when the airflow becomes detached from the wing surface. Increasing camber also exposes more of the wing area to the airflow, so drag is expected to increase with increasing camber. I estimated camber height as the perpendicular distance of the patagium point from the chord line (Fig. 3B). I define relative camber here as the ratio of the camber height to the chord length. Relative camber corrects for overall size when comparing wings of different individuals and/or species.

All limb positions of the animals other than angle of attack and camber were defined with respect to the animal-centered coordinate system, to separate movements of the limbs from the overall movements of the animal.

The angle of attack of the wing depends on both the angle of the body with respect to the glide trajectory and the position of

the limbs with respect to the body. Of these components of angle of attack, the one over which a gliding animal has the most direct control is the angle of the chord line with respect to the body, which I am calling the chord angle. I computed chord angle as the projection on the *x*–*y* (sagittal) plane of the angle between a line connecting the wrist and ankle and the body plane. This angle is significant aerodynamically because changes in this angle represent a movement of the limbs that tends to change the angle of attack of the wing.

The elevation of the wingtips above the body, or dihedral, affects the passive stability of a flying body (Bertin, 2002). The elevation angle is here defined as the projection on the *y*–*z* (transverse) plane of the angle between a line connecting the sternum and wrist and the *z* (mediolateral) axis. I consider the elevation angle to be zero when the wrist is vertically even with the body plane. A positive angle indicates that the forelimbs are held above the plane of the body, i.e. at a dihedral, whereas a negative angle indicates that the forelimbs are held below the plane of the body, which is called an anhedral.

Protraction is defined as movement of a limb toward the head. The protraction angle is here defined as the projection on the *x*–*z* (frontal) plane of the angle between a line connecting the sternum and wrist and the *z* (mediolateral) axis. I consider the protraction angle to be zero when the forelimb is perpendicular to the body axis as seen from a dorsal view, and positive when the forelimb moves toward the head. This angle is analogous to the sweep angle of an airplane wing, which affects its lift-generating performance (Bertin, 2002). A positive protraction angle indicates a forward-swept wing, whereas a negative protraction angle means the wing is swept backward.

For each time step, I estimated the area of a single wing by taking the mean of the 3D distance between the sternum and wrist and the 3D distance between the pelvis and the ankle and multiplying it by the chord length computed for that time step, and doubled this quantity to estimate the total wing area. I computed the wing loading by dividing the weight of the animal measured just before the trial (mass × acceleration due to gravity) by the estimated wing area. Errors inherent in using this estimate will affect the exact values of wing loading and force coefficients. However, there is no bias in this estimator that affects comparisons among individuals, and use of this approach allows direct comparisons with earlier studies.

Statistics

Means are reported ± 1 standard deviation (s.d.). Correlations between the average value of variables over the glide sequence were estimated using Pearson correlation coefficients with a significance level P=0.05. When more than one factor is predicted to have an effect, I used a stepwise multiple regression analysis, also with a significance level P=0.05, to estimate the effect of each of the factors while holding the others constant. Multiple regressions were done using average values for each glide sequence. To account for intra-individual variation, regressions were performed separately on each individual. This approach gave results consistent with those for the individuals combined (data not shown).

To estimate correlations between variables within a glide sequence I used cross correlation analysis (Chatfield, 1992). Cross correlation is a technique that estimates the correlation between two sets of time series data, taking into account that the correlation may not be instantaneous. The correlation is computed at a number of positive and negative time lags and the lag with the maximum absolute value for the correlation coefficient is taken to be the true time lag for the relationship. This technique does not assume a causal relationship between the two variables. For the cross correlation, data were smoothed using a lowpass Butterworth filter with a cut-off frequency of 25 Hz and the mean value for the trial was subtracted from each data point to remove the effect of overall trends (detrended) before computing the cross correlation functions (Fry, 1993). The cut-off frequency was selected based on visual inspection of the raw data along with the filtered data and chosen based on the elimination of point-to-point variation while maintaining overall trends. A sensitivity analysis indicated that varying the cut-off frequency by ± 5 Hz does not affect the conclusions based on the cross correlation. 95% confidence limits (CL) were estimated at each time lag as:

$$\mathrm{CL} = \pm 2/\sqrt{N}\,, \tag{9}$$

where N is the number of frames used at that time lag (Fry, 1993).

Results

Body posture

The angles of attack used during gliding were high, with a mean of 44.2±3.1° (Table 1, Fig. 4). Relative camber had a

Table 1. *Summary of descriptive statistics and ANOVA results*

	P. breviceps	*G. volans**	Combined	*F*, d.f.=1	*P*
Wing loading (N m^{-2})	30.30±5.07	45.33±5.46	36.30±8.74	158.276	<0.001
X acceleration (m s^{-2})	2.1±0.6	2.9±0.9	2.4±0.8	25.869	<0.001
Y acceleration (m s^{-2})	–1.0±0.5	–2.5±1.1	–1.6±1.0	87.993	<0.001
Lift coefficient	1.48±0.18	2.12±0.46	1.72±0.44	84.9	<0.001
Drag coefficient	1.07±0.13	0.98±0.20	1.04±0.16	7.231	0.009
Lift-to-drag ratio	1.39±0.16	2.26±0.68	1.72±0.61	81.91	<0.001
Angle of attack (deg.)	44.2±3.1	42.49±4.51	43.53±3.77	4.165	0.044
Relative camber	0.09±0.02	0.135±0.017	0.100±0.032	81.66	<0.001
Glide angle (deg.)	49.6±2.5	47.56±5.03	48.83±3.75	6.453	0.013
Velocity (m s^{-1})	5.08±0.30	5.11±0.19	5.09±0.26	0.415	0.521

Values are means ± s.d. *P. breviceps*, N=55; *G. volans*, N=33.
*Data for *G. volans* from (Bishop, 2006).

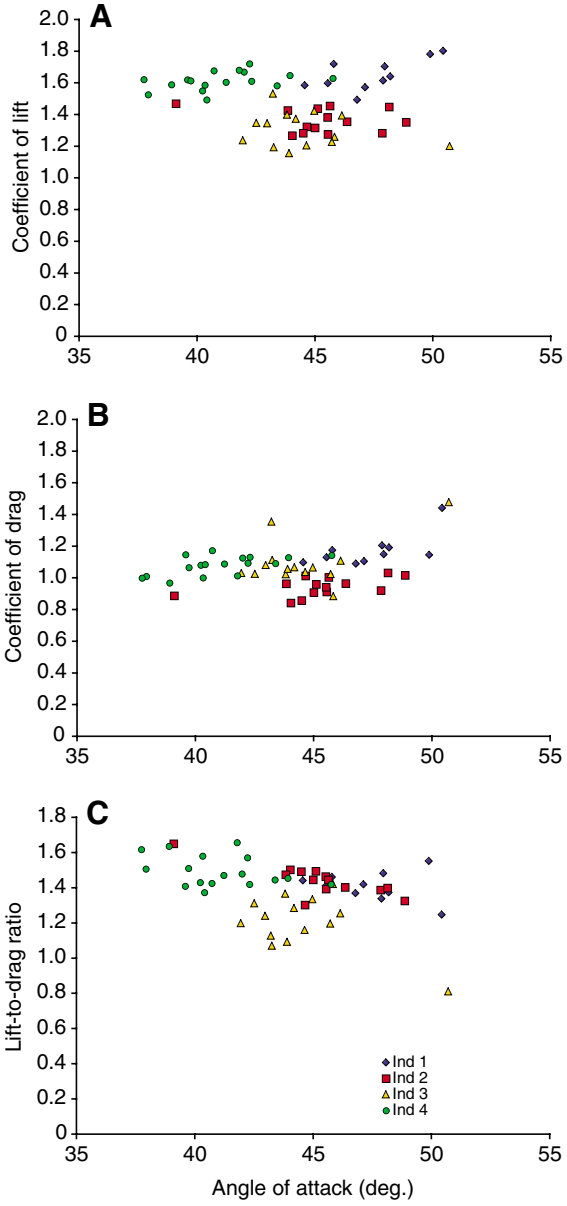

Fig. 4. (A) Coefficient of lift, (B) coefficient of drag, and (C) lift-to-drag ratio *vs* angle of attack. The range of lift coefficients used by each glider is similar, although they used different ranges of angles of attack. No correlation was detected between lift coefficient and angle of attack. There appears to be no correlation between angle of attack and drag, but a multiple regression analysis detected a significant positive relationship. Multiple regression analysis detected a significant negative correlation between angle of attack and lift-to-drag ratio. Points represent averages over a glide sequence for 4 animals (Ind1–4).

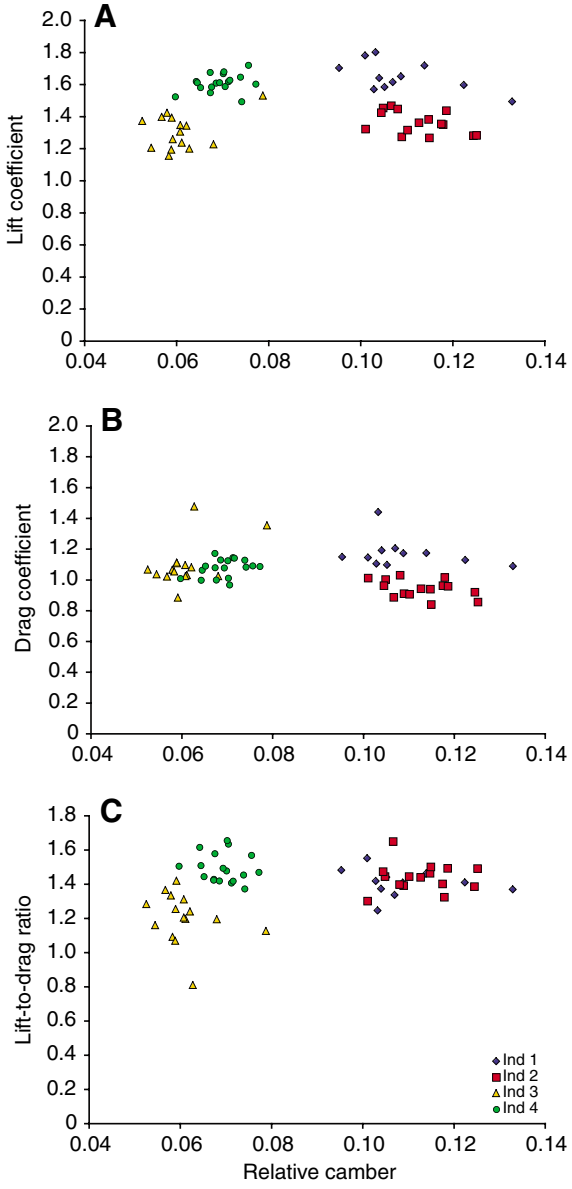

Fig. 5. (A) Coefficient of lift, (B) coefficient of drag, and (C) lift-to-drag ratio *vs* relative camber. Individual gliders use different ranges of relative camber. There was no significant correlation between relative camber and lift coefficient. Although no correlation is apparent between drag coefficient and relative camber, multiple regression results detected a significant negative correlation. There is a significant positive correlation between lift-to-drag ratio and relative camber. Points represent averages over a glide sequence for 4 animals (Ind1–4).

mean of 0.09±0.02 (Table 1, Fig. 5), indicating that on average camber height was 9% of the chord length.

Overall, the wing tended to be held in a position that increased its angle of attack compared to that determined by the pitch of the body (Table 2). The chord angle with respect to the body plane averaged over the glide sequence was positive in all but one trial, with a mean for all trials of 15.2±6.7°. In 35 of the 49 trials, the chord angle remained positive throughout the glide sequence (Fig. 6A). In the remaining 14 trials, chord angles started out small and positive and became negative in the last half of the glide sequence.

When averaged over a glide sequence, the forelimb tended to be held in a slightly elevated (wrist higher than the body plane) posture in most cases. The mean elevation angle for all trials was 6.7±7.8° (Table 2). There was one individual who used much higher positive elevation angles than the rest, but the more typical pattern was to hold the forelimb fairly close to horizontal with respect to the body plane. In the majority of video

Table 2. *Summary statistics for limb positions in P. breviceps*

Limb position	Mean	Minimum	Maximum
Angle of attack (deg.)	43.4±2.9	37.7	50.7
Relative camber	0.08±0.02	0.05	0.13
Chord angle (deg.)	15.2±6.7	–1.4	32.7
Elevation angle (deg.)	6.7±7.8	–5.8	32.3
Protraction angle (deg.)	30.6±5.4	14.7	46.3

Values are means ± s.d., *N*=49.

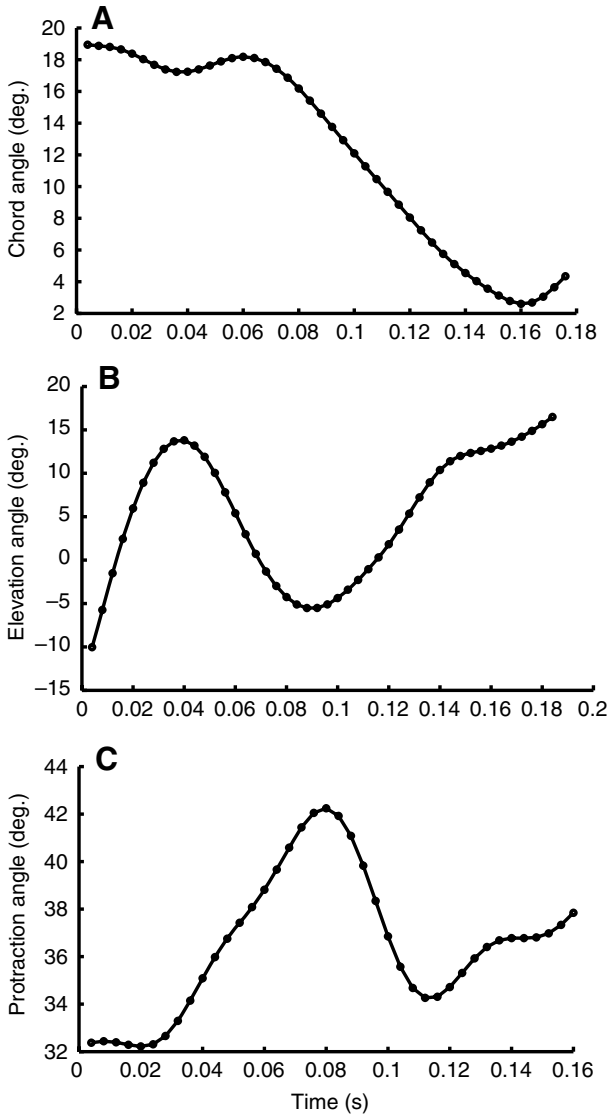

Fig. 6. Limb positions *vs* time for separate representative glide sequences. Limb movements were ubiquitous throughout all glides and of magnitudes that far exceed the estimated digitizing error. The correlation between these movements and body rotations indicate that these movements function to control body orientation. (A) Chord angles tended to be fairly large and positive at the start of the sequences and decrease through the trial. Chord angles became negative in 14 of 49 trials. (B) Forelimb elevation angles tended to fluctuate between positive and negative, but usually remained fairly small. (C) Forelimb protraction angles were large and positive at all times in all glide sequences.

sequences, the elevation angle changed from positive to negative, or the reverse, at least once (Fig. 6B).

The forelimbs were kept in a strongly protracted position for all glides, at no time in any glide was the wrist observed to be posterior to the sternum (Fig. 6C). The mean protraction angle over all trials was 30.6±5.4° (Table 2).

Gliding performance

The resultant velocities used by the sugar gliders had a mean of 5.08±0.30 m s^{-1}. In 54 of 55 cases the gliders accelerated in the forward direction with an average horizontal acceleration of 2.1±0.6 m s^{-2}. The downward accelerations were small, with a mean of 1.0±0.5 m s^{-2}. This corresponds to an average upward acceleration due to aerodynamic forces (i.e. with gravity subtracted) of 8.8 m s^{-2} (Table 1).

The observed glides were fairly steep, with a mean glide angle of 49.6±2.5° (Table 1). The glide angles decreased over the captured glide sequence in nearly all of the glides, indicating that the animals were flattening their glide trajectory at this point in the glide. The mean rate of change in the glide angle was –11.1±5.6° s^{-1}. Only two glides had glide angles that increased over the captured glide sequence. There was a small, but significant correlation between downward acceleration and the rate of decrease in the glide angle (r=–0.276, P=0.042).

Relationship between limb position and aerodynamic forces

In general, the sugar gliders produced more lift than drag. The lift coefficients averaged 1.48±0.18 (Table 1). The mean drag coefficient for all trials was 1.07±0.13 (Table 1). The mean lift-to-drag ratio was 1.39±0.16 (Table 1). All of the gliders performed similarly in terms of lift and drag production, although they did not all use the same range of angles of attack (Fig. 4) or camber (Fig. 5).

It should be noted that lift and drag are affected by multiple factors; angle of attack and camber are both likely to contribute to the production of aerodynamic forces. Therefore, a simple relationship between forces and any one factor is difficult to interpret from a graphical representation and multiple regression techniques must be used to control for the effects of the other factors. However, graphs are provided to illustrate the range and magnitude of these variables. Examination of Fig. 6 and Fig. 7 suggests that there was little to no relationship between either angle of attack or camber with lift coefficient, drag coefficient, or lift-to-drag ratio. This was supported in the case of lift coefficient by a stepwise multiple regression analysis (Table 3), which removed both angle of attack and relative camber from the model as factors affecting lift.

Multiple regression analysis for drag, however, retained both angle of attack and relative camber as significant factors (Table 3). A model that included only angle of attack accounted for only 6.2% of the variation in drag coefficient, but together with relative camber accounted for 24% of the variation in drag. In the model including both angle of attack and relative camber, angle of attack was strongly positively correlated with drag, whereas relative camber was strongly negatively correlated with drag.

Similarly, for lift-to-drag ratio, angle of attack on its own accounted for only 12.8% of the variation in lift-to-drag ratio, but a model including both angle of attack and camber

accounted for 41.1% (Table 3). This model indicates a strong negative correlation between angle of attack and lift-to-drag ratio and a strong positive correlation between relative camber and lift-to-drag ratio.

Relationship between aerodynamic forces and performance

Glide angle was strongly related to both wing loading and to the production of lift (Fig. 7). A stepwise multiple regression removed drag coefficient as a factor contributing to glide angle and retained lift coefficient and wing loading (Table 3). Wing loading alone accounted for 68.1% of the variation in glide angle and wing loading and lift coefficient together accounted for 80.9%. The model including both wing loading and lift coefficient shows that wing loading was very strongly positively correlated with glide angle, indicating that heavier wing loading produced steeper instantaneous glide angles, and lift coefficient was negatively correlated with glide angle, in keeping with the expectation that more lift produces a shallower glide.

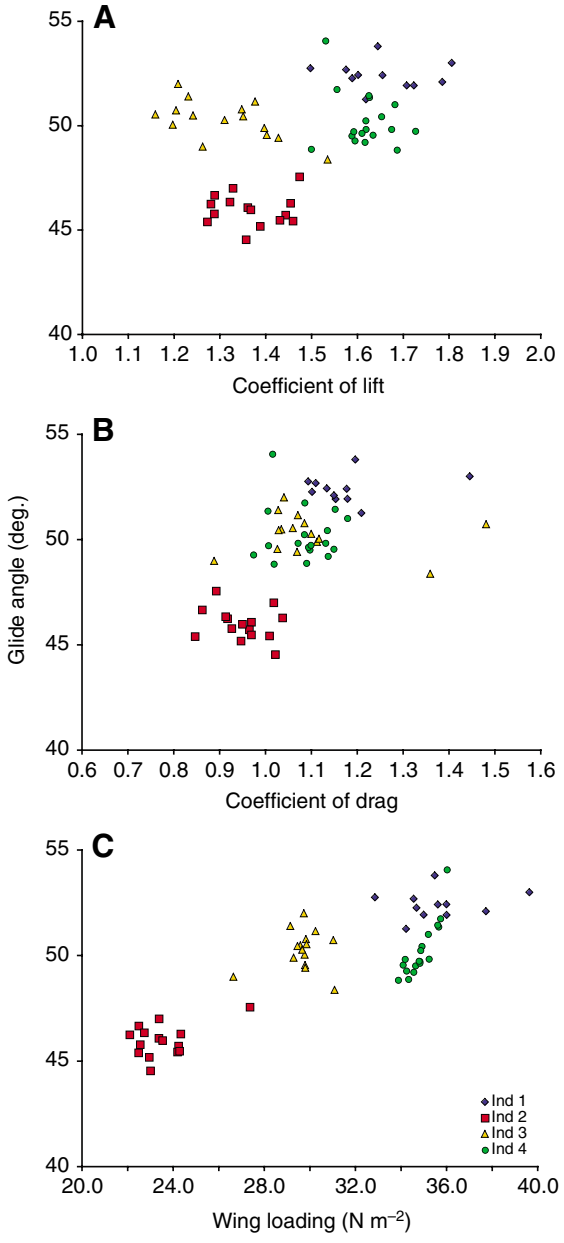

Fig. 7. Glide angle *vs* (A) coefficient of lift, (B) coefficient of drag, and (C) wing loading. There appears to be no relationship between glide angle and lift coefficient, but multiple regression detects a significant negative correlation. There is no correlation between drag coefficient and glide angle. There is a clear positive relationship between glide angle and wing loading. N=4 animals (Ind1–4).

Velocity was affected by both wing loading and aerodynamic force production (Fig. 8). A stepwise multiple regression analysis retained wing loading, lift coefficient and drag coefficient as factors contributing to velocity (Table 3). Wing loading alone accounted for 57.2% of the variation in velocity, wing loading and lift coefficient together accounted for 75.0% and wing loading, lift coefficient and drag coefficient accounted for 79.3%. Wing loading was strongly positively correlated with velocity, whereas lift and drag coefficients were both negatively correlated with velocity. This is consistent with aerodynamic theory, which predicts that more heavily wing-loaded animals will glide faster (Norberg, 1990) and that at steep glide trajectories, both lift and drag contribute to the force opposing gravity and will tend to slow the animal down.

Relationship between limb position and rotations

The results of the cross correlation analysis between limb movements and body rotations are presented for both the pooled data set including all of the individuals, and also each individual considered separately. Because one of the body markers was lost during data collection on Ind 1, body rotations were analyzed in only four trials for that individual. Due to the very small sample size, this individual is omitted from the analysis of individual results, but is incorporated into the pooled data. These results are summarized in Table 4. For more information

Table 3. *Stepwise multiple regression results*

	Beta coefficient	P	Adjusted R^2
Lift coefficient			
Angle of attack			
Relative camber			
Drag coefficient			0.24
Angle of attack	0.528	<0.001	
Relative camber	–0.499	0.001	
Lift-to-drag ratio			0.411
Angle of attack	–0.684	<0.001	
Relative camber	0.618	<0.001	
Glide angle			0.809
Lift coefficient	–0.541	<0.001	
Drag coefficient			
Wing loading	1.233	0.001	
Velocity			0.793
Lift coefficient	–0.684	<0.001	
Drag coefficient	–0.278	0.001	
Wing loading	1.449	<0.001	

Adjusted R^2 is for the model as a whole.

No reported value indicates that the covariate was excluded by the stepwise regression model.

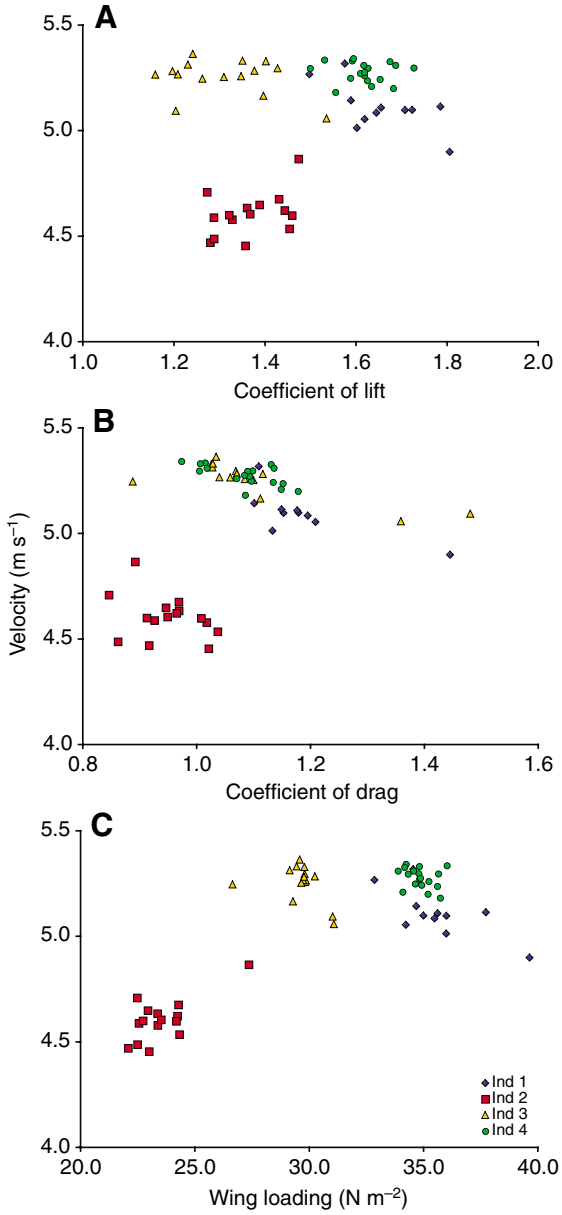

Fig. 8. Velocity *vs* (A) coefficient of lift, (B) coefficient of drag, and (C) wing loading. Multiple regression detects a significant negative correlation between both lift and drag coefficients and velocity. Wing loading has a positive relationship with velocity. *N*=4 animals (Ind1–4).

on the magnitudes of the correlation coefficients and time lags for selected trials, please see Figs S1–S3 in supplementary material.

Pitch

There were no limb positions that had significant correlations with pitch in more than 70% of the trials for all of the gliders pooled, but there were strong associations for the individuals taken separately.

For Ind 2, there was a significant positive correlation between pitch and chord angle in 79% of trials, indicating that nose-up rotations in pitch were associated with movements of the limbs that tend to increase the angle of attack. For the trials with significant positive correlations, the lags at which the maximum correlation coefficients occurred were mostly zero and positive, with small negative lags in two out of 14 total trials for this individual. In this and all subsequent comparisons, a positive lag indicates that changes in limb position led changes in rotations and negative lags mean that changes in rotation led changes in limb position.

Table 4. *Summary of cross correlation results*

	Limb position	Correlation	Lag
Pitch			
All	None		
Ind 2	Chord angle	Positive	Zero/positive
Ind 3	Chord angle	Positive	Zero
	Protraction	Negative	Positive
Ind 4	Relative camber	Negative	Positive
	Protraction	Negative	Positive
Roll			
All	Chord angle	Positive	Zero/positive
	Elevation angle	Positive	Zero/positive
Ind 2	Chord angle	Positive	Zero/positive
	Elevation angle	Positive	Positive
Ind 3	Elevation angle	Positive	Zero
Ind 4	Relative camber	Negative	Zero/negative
Yaw			
All	Protraction	Negative	Zero/negative
Ind 2	Relative camber	Negative	Zero/positive
	Protraction	Negative	Zero/negative
Ind 3	None		
Ind 4	Protraction	Negative	Zero/negative
	Chord angle	Negative	Negative
	Elevation angle	Negative	Negative

Ind 2–4, individual animals.

Rotations and limb positions are reported as being correlated if they had significant correlations in the same direction (positive or negative) in at least 70% of the trials.

For Ind 3, pitch had significant correlations with chord angle and protraction. Chord angle had a significant positive correlation with pitch in 79% of 14 trials, indicating that nose-up rotations in pitch were associated with movements that tend to increase angle of attack. In trials with significant positive correlations, the maximum correlation coefficients occurred mostly at a lag of zero, with the exception of two trials, one with a lag of 2 and one of –3. There was a significant negative correlation between pitch and forelimb protraction in 71% of trials for this individual, indicating that movements of the forelimb toward the head were associated with nose-down changes in pitch. Of the trials for this individual with significant negative correlations, the maximum correlation occurred at positive lags in most trials, but one trial had a lag of zero and three had negative lags.

In Ind 4, pitch was most often correlated with relative camber and protraction. There was a significant negative correlation between pitch and relative camber in 76% of the 17 trials for this individual, such that nose-up pitching rotations were associated with decreases in camber. For trials with significant

negative correlations, the lags for the maximum correlation were mostly large and positive, ranging from 3–10, with the exception of three with large negative lags. Protraction was significantly negatively correlated with pitch in 71% of the trials for this individual, indicating that nose-up rotations were associated with movements of the forelimbs away from the head. For trials with a significant correlation, the lags were mostly positive, with one zero lag and two trials with negative lags.

Roll

For all trials pooled there were strong associations of both chord angle and elevation angle with roll. In 71% of trials there was a significant positive correlation between chord angle and roll, indicating that movements of the limbs that tend to increase the angle of attack on the left side were associated with rolling rotations to the left (right hip higher than the left). When correlations were positive, lags were mostly zero and positive, but six of the 35 trials had small negative lags. Limb elevation had a significant positive correlation with roll in 76% of all trials, indicating that movements of the limbs above the plane of the body on the left were associated with rolling rotations to the left. For trials with a significant positive correlation, most of the lags were zero or small and positive (up to three), but three trials had small negative lags. Ind 2 showed the same correlations as the pooled data. Roll was positively correlated with limb elevation and forelimb protraction in Ind 3, but not with chord angle.

In Ind 4 there was a very strong association between relative camber and roll. Roll and relative camber had a significant negative correlation in 94% of the trials for this individual, meaning that increases in camber on the left were associated with rolling rotations to the right. Lags were mostly small and negative, up to –3; five trials had a lag of zero, and one had a positive lag of one.

Yaw

There was a tendency in the pooled data set for yaw to be associated with protraction of the forelimb. In 76% of trials protraction was significantly negatively correlated with yaw angle, indicating that yawing rotations to the right were associated with movement of the left forelimb away from the head. In trials with significant negative correlations, lags were either zero or small and negative, with the exception of four trials with small positive lags ($\leqslant$3) and one with a lag of nine. This trend was driven primarily by Ind 2 and Ind 4, who had a significant negative correlation between protraction and yaw in 79% and 100% of their trials, respectively.

In Ind 2 there was a significant negative correlation between yaw and relative camber in 86% of trials, all with zero or small positive lags. This indicates that increases in camber on the left were associated with yawing rotations to the left. This individual had no strong associations between yaw and any other limb position.

In addition to protraction, Ind 4 also showed strong associations of yaw with both chord angle and limb elevation. This individual had a significant negative correlation between yaw and chord angle in 71% of trials, indicating that movements of the limbs that tend to increase angle of attack on the left were associated with yawing rotations to the left; all trials with significant negative correlations had negative lags ranging from –10 to –2. Wing elevation was significantly negatively correlated with yaw in 82% of trials for this individual, indicating that movements of the forelimbs above the plane of the body on the left were associated with yawing rotations to the left, all with negative lags (ranging from –9 to –4).

Discussion

Limb movements and body rotations

To maintain a steady trajectory and avoid tumbling or spinning out of control, a glider must correct any inadvertent perturbations that cause body rotations. Conversely, in order to execute deliberate maneuvers, a glider must be able to initiate these rotations, and then restore equilibrium. The cross correlation results strongly suggest that sugar gliders employ limb movements extensively to control body rotations. If they did not, there would either have been no significant correlation between limb movements and body rotations at any time lag, or there would have been no bias toward either positive or negative correlation coefficients. Although directional biases in correlation coefficients appear weak for all of the gliders pooled, when examined individually there were strong biases toward correlations in a particular direction (Table 4). This indicates that the individual gliders used different limb movements to control the same body rotations. This is the first time such individual variation in gliding behavior has been documented.

Body rotations result from asymmetrical generation of forces across the respective body axes. In addition, rotations can be induced by inertial effects when the position of the center of mass changes due to movement of the limbs. I estimated the moment of inertia of the gliders by dividing frozen cadaver specimens of sugar gliders into 1 cm sections in both the longitudinal and transverse directions and weighing each segment. The estimated moments of inertia were very small, 1.4×10^{-5} kg m^2 for the roll axis and 9.9×10^{-5} kg m^2 for the pitch and yaw axes, so these body rotations are expected to be very sensitive to changes in force at the wings. Therefore, the very short lag times reported here are credible.

Although this analysis of the relationships between limb movements and body rotations provides valuable insights, there are some limitations that should be noted. First, the captured glide sequences are shorter than the oscillation period of the limb movements and body rotations. This means that the lag at which the actual maximum correlation occurs may be greater than the number of lags tested, in which case it would not be detected. Because these tend to be oscillating phenomena, there are alternating positive and negative peaks in the cross correlation function that decrease with increasing distance from the actual time lag of the function. If the actual time lag is greater than the number of lags tested, it is likely that the next highest correlation coefficient will have the opposite sign. These errors are most likely to have occurred where the absolute value of the actual lag is high, because nearby lower correlation peaks are more likely to be detected when correlation maxima have small or zero lags, verifying that it is a true maximum. It should be noted that errors resulting from the short length of the video sequences are conservative because there is a tendency to miss

significant correlations rather than to detect false correlations, and that analysis of longer glide sequences would be expected to yield even stronger correlations.

Another limitation to this approach is that cross correlation analysis does not take into account the interaction between the effects of multiple limb movements on each body rotation. Different limb movements can produce force asymmetries that will result in a single kind of rotation, therefore it is possible that some correlations were missed due to these interactive effects. A related limitation is that only one wing was marked and the effect of the position of one wing on body rotations depends entirely on what the opposite wing is doing. I make the conservative assumption here that the opposite wing is stationary; it is likely that even stronger correlations would be detected if measurements had been taken from both wings.

Gliding performance

Glide angle

The glides performed by the sugar gliders were quite steep. Glide angles of sugar gliders averaged over whole glides in the wild have been estimated to be 29.69±1.10° (mean ± s.e.m., N=13) (Jackson, 2000), while the gliders in this study used glide angles around 50°. This is probably due to the fact that gliders launched from a relatively low height and did not have time to reach their minimum glide angle, or that they chose a glide angle according to their intended target. It is interesting to note that the vertical accelerations were very small, indicating that the gliders were generating nearly enough aerodynamic force to balance their weight at this point in the glide, and their glide angles were rapidly decreasing.

Glide angle is geometrically defined by the ratio of vertical velocity to horizontal velocity. Assuming similar launch velocities, the horizontal and vertical velocities at a given time after the launch are determined by the horizontal and vertical accelerations since launching, which are in turn determined by the horizontal and vertical forces. For a given lift and drag coefficient, a more heavily wing-loaded animal will have a greater vertical acceleration (and therefore velocity) at a similar time in the glide than one with lower wing loading because its weight is greater relative to the aerodynamic force it produces, and it will therefore glide more steeply. The findings of this study are consistent with this prediction. Glide angle was strongly associated with wing loading (Table 3), such that animals that were heavier relative to their wing size had steeper instantaneous glide angles.

Velocity

Glide velocity depends on both wing loading and aerodynamic forces. The body weight of the animal is supported by the vertical component of a resultant aerodynamic force, which is the vector sum of lift and drag. The resultant aerodynamic force is given by:

$$R = \tfrac{1}{2}(\rho V^2 C_{\mathrm{R}} S)\,, \tag{10}$$

where R is the resultant aerodynamic force, ρ is the density of air, V is the glide velocity, C_{R} is a dimensionless force coefficient and S is the planform area of the animal. In a steady, non-accelerating glide the resultant aerodynamic force is equal to the animal's body weight. Substituting body weight for the resultant aerodynamic force and solving for velocity gives:

$$V = \sqrt{\frac{2Mg}{\rho C_{\mathrm{R}} S}}\,, \tag{11}$$

where M is body mass and $\boldsymbol{g}$ is acceleration due to gravity. From this equation we see that wing loading ($M\boldsymbol{g}/S$) is directly proportional to the square of glide velocity. Because both lift and drag are also proportional to the square of velocity, more heavily wing-loaded animals must fly faster to generate enough aerodynamic force to balance their body weight. We can also read from this equation that to minimize glide velocity, an animal should maximize its resultant aerodynamic force coefficient. At steep glide angles, both lift and drag make substantial contributions to the resultant aerodynamic force, so generating high lift and drag coefficients reduces glide velocity.

The results of this study conform well to these predictions. Wing loading had a strong positive correlation with velocity (Table 3), indicating that more heavily wing-loaded sugar gliders do, in fact, glide faster than those with lower wing loading. In addition, lift and drag coefficients were negatively correlated with glide velocity (Table 3). A higher lift coefficient means that more lift is generated for a given velocity and wing area, and the same is true for drag coefficient. This means that with higher force coefficients, the amount of force needed to support the body weight is achieved at a lower speed.

Comparison with flying squirrels

By making comparisons of the gliding behavior and performance of diverse groups of gliding mammals, we can begin to discover general rules for mammalian gliding. Studies that link the details of gliding kinematics with ecologically important performance variables are instrumental in providing a mechanistic basis for such rules. McGuire and Dudley (McGuire and Dudley, 2005) made an interspecies comparison of gliding performance in closely related gliding lizards, examining the effect of body size on gliding performance in nearly isometrically scaled lizards. In addition, Socha and LaBarbera (Socha and LaBarbera, 2005) examined the effect of body size on gliding performance in tree snakes of different ages in the same species. To date, there have been no interspecies comparisons investigating convergence in gliding behavior.

A comparison with a study of southern flying squirrels (*Glaucomys volans*) under conditions similar to those in this study (Bishop, 2006) shows that both species exhibit similar gliding performance in terms of glide velocity, but sugar gliders had significantly higher glide angles than flying squirrels (Table 1). Sugar gliders also used significantly higher angles of attack than flying squirrels, whereas flying squirrels used significantly greater amounts of relative camber than sugar gliders (Table 1).

Flying squirrels generated more lift and less drag than sugar gliders. Despite large differences in lift and drag production between flying squirrels and sugar gliders, their glide angles were remarkably similar, indicating that the squirrels did not use the additional lift to flatten their glide trajectory during this phase of the glide, but rather to accelerate horizontally (Table 1). Flying squirrels had both greater horizontal and

vertical accelerations than sugar gliders, but had velocities during the captured portion of the glide that were statistically indistinguishable from those of sugar gliders (Table 1). This suggests that flying squirrels would ultimately reach a higher glide velocity than sugar gliders, as expected based on their greater wing loading (Table 1).

There are several possible reasons why flying squirrels tend to produce greater lift coefficients than sugar gliders. One is that their wings are more cambered in flight (Table 1). In addition, flying squirrels possess a well-developed forewing structure called a propatagium that is present, but much smaller, in sugar gliders. This flap of skin anterior to the forelimb attaches distally at the pollex and proximally at the zygomatic arch on the cheek in flying squirrels (Johnson-Murray, 1977), but only extends from the neck to the center of the antebrachium in sugar gliders (Johnson-Murray, 1987). It is possible that this structure behaves as a leading edge flap which, when deflected downward, enhances the camber of the wing and can also help to delay stall at high angles of attack (Wilkinson et al., 2006).

Glide velocity was related to both force production and wing loading in the sugar gliders in a manner consistent with conventional aerodynamic theory. More heavily wing-loaded animals tended to have faster glides, and greater production of aerodynamic forces (both lift and drag components) tended to result in slower glides. In flying squirrels, however, velocity was positively correlated with lift coefficient, but not correlated with either drag coefficient or wing loading. If the glides were steady, one would expect a negative correlation between velocity and lift coefficient (Eqn 4). This result is explained by the fact that in the flying squirrels high lift coefficients were associated with horizontal acceleration, rather than simply balancing the body weight. In the case of the squirrels, increasing the lift coefficient increased the forward acceleration, which in turn contributed to greater overall velocity.

Conclusions

Although it may be very important in certain circumstances to travel as far as possible, if an animal cannot control its body orientation and trajectory well enough to arrive safely at a desired location, optimizing glide distance does not do much good. Although more information is needed on the effect of limb movements on flight performance, particularly oscillations intermediate in amplitude between the small ones seen in this study and those seen in powered flight, models of the origin of flapping flight should not focus solely on the generation of lift and thrust forces without taking into account the role of stability and maneuverability. This study suggests that limb movements are used differently by individual gliders to control body rotations, so movements in all orientations should be considered when investigating the effects of these intermediate amplitude limb movements, and not focus solely on dorsoventral 'flapping'.

It is possible that small amplitude movements of the wings, like those found in this study, which came about primarily for the purpose of maintaining stability, may have secondarily increased lift generation (Norberg, 1985) or thrust (Vandenberghe et al., 2004), and could have improved other components of glide performance such as glide angle or velocity. Studies of low aspect ratio wings at Reynolds numbers relevant to vertebrate flight have shown that up to aspect ratios of ~2, aerodynamic performance declines with increasing aspect ratio, particularly at the high angles of attack used by the gliders in this study (Torres and Mueller, 2001; Shyy et al., 2005). But, at higher aspect ratios, aerodynamic performance increases with increasing aspect ratio. This may have presented a kind of adaptive barrier during the transition from a low aspect ratio glider wing to a high aspect ratio bat wing. It is possible that limb movements leading to flapping behavior provided the means for overcoming this transition between aerodynamic regimes. Understanding the relationships between kinematics, force production and gliding performance across species in the context of disparate performance parameters, not only improves our understanding of and appreciation for gliding as a form of locomotion, but will also lead to more fruitful hypotheses regarding the origin of flight in bats.

List of abbreviations and symbols

ap	length of anterior segment of patagium
α	angle of attack
$\mathbf{C}$	chord vector
C_D	coefficient of drag
C_F	coefficient of resultant aerodynamic force
C_L	coefficient of lift
CL	confidence limit
D	drag
φ	reference angle between drag and resultant aerodynamic force
$\boldsymbol{g}$	acceleration due to gravity
h	camber height
L	lift
M	mass
ϕ	reference angle between anterior patagium segment and chord line
$\mathbf{R}$	resultant aerodynamic force vector
R	resultant aerodynamic force
ρ	air density
S	wing area
θ	glide angle
$\mathbf{V}$	velocity vector
V	velocity magnitude
X,Y,Z	global coordinates
x,y,z	animal-centered coordinates

I am very grateful to A. Kinney, A. Sullivan, K. Kuchenbecker, A. Roemer, A. Berg, A. Clifford, B. Moore, and R. Heine for assistance with animal training and data collection. A huge thank-you to T. Hedrick for extensive help with data analysis and valuable comments on this manuscript. Help with statistics was graciously provided by J. Iriarte-Diaz and E. vonWettberg. The beauty and clarity of the figures were greatly enhanced by glider illustrations by M. Houllahan. This work was greatly improved by discussion and comments from S. Swartz, S. Gatesy, K. Breuer, E. Brainerd, J. Witman, A. Biewener, G. Spedding, K. Metzger, T. Hseih, J. Hamilton, F. Nelson, A. Clifford, R. Mehta, E. vonWettberg and three anonymous reviewers. Thanks to A. Biewener and the staff and Concord Field Station for providing access to their facilities. This work was supported by NSF DDIG IBN-0407899.

References

Bertin, J. J. (2002). *Aerodynamics for Engineers*. Delhi: Pearson Education.

Bishop, K. L. (2006). The relationship between 3D kinematics and gliding performance in the southern flying squirrel, *Glaucomys volans. J. Exp. Biol.* **209**, 689-701.

Bock, W. J. (1965). The role of adaptive mechanisms in the origin of higher levels of organization. *Syst. Zool.* **14**, 272-287.

Caple, G., Balda, R. P. and Willis, W. R. (1983). The physics of leaping animals and the evolution of preflight. *Am. Nat.* **121**, 455-476.

Chatfield, C. (1992). *The Analysis of Time Series: An Introduction*. London, New York: Chapman & Hall.

Clark, B. D. (1978). Energetics of hovering flight and the origin of bats. In *Major Patterns in Vertebrate Evolution* (ed. M. K. Hecht, P. C. Goody and B. M. Hecht), pp. 423-425. New York: Plenum.

Emerson, S. B. and Koehl, M. A. R. (1990). The interaction of behavioral and morphological change in the evolution of a novel locomotor type: 'flying' frogs. *Evolution* **44**, 1931-1946.

Endo, H., Yokokawa, K., Kurohmaru, M. and Hayashi, Y. (1998). Functional anatomy of gliding membrane muscles in the sugar glider (*Petaurus breviceps*). *Ann. Anat.* **180**, 93-96.

Fry, J. C. (1993). *Biological Data Analysis: A Practical Approach*. New York: Oxford University Press.

Galvao, R., Israeli, E., Song, A., Tian, X., Bishop, K. L., Swartz, S. and Breuer, K. (2006). The aerodynamics of compliant membrane wings modeled on mammalian flight mechanics. Proceedings of the 36th AIAA Fluid Dynamics Conference, June 2006. AIAA Paper 2006-2866. Reston, VA: AIAA.

Jackson, S. M. (2000). Glide angle in the genus *Petaurus* and a review of gliding in mammals. *Mammal Rev.* **30**, 9-30.

Johnson-Murray, J. L. (1977). Myology of the gliding membranes of some petauristine rodents (genera: *Glaucomys*, *Pteromys*, *Petinomys*, and *Petaurista*). *J. Mammal.* **58**, 374-384.

Johnson-Murray, J. L. (1987). The comparative myology of the gliding membranes of *Acrobates*, *Petauroides* and *Petaurus* contrasted with the cutaneous myology of *Hemibelideus* and *Pseudocheirus* (Marsupialia: Phalangeridae) and with selected gliding Rodentia (Sciuridae and Anamoluridae). *Aust. J. Zool.* **35**, 101-113.

McCay, M. G. (2001a). Aerodynamic stability and maneuverability of the gliding frog *Polypedates dennysi. J. Exp. Biol.* **204**, 2817-2826.

McCay, M. G. (2001b). The evolution of gliding in neotropical tree frogs. PhD thesis, University of California, Berkeley, USA.

McGuire, J. A. and Dudley, R. (2005). The cost of living large: comparative gliding performance in flying lizards (Agamidae: Draco). *Am. Nat.* **166**, 93-106.

Norberg, U. M. (1985). Evolution of vertebrate flight: an aerodynamic model for the transition from gliding to active flight. *Am. Nat.* **126**, 303-327.

Norberg, U. M. (1990). *Vertebrate Flight: Mechanics, Physiology, Morphology, Ecology and Evolution*. Berlin, Heidelberg: Springer-Verlag.

Padian, K. (1982). Running, leaping, lifting off. *Sciences New York* **22**, 10-15.

Parkes, K. C. (1966). Speculations on the origin of feathers. *Living Bird* **5**, 77-86.

Shyy, W., Ifju, P. and Viieru, D. (2005). Membrane wing-based micro air vehicles. *Appl. Mech. Rev.* **58**, 283-301.

Simmons, N. B. (1995). Bat relationships and the origin of flight. *Symp. Zool. Soc. Lond.* **67**, 27-43.

Smith, J. D. (1976). Comments on flight and the evolution of bats. In *Major Patterns in Vertebrate Evolution* (ed. M. K. Hecht, P. C. Goody and B. M. Hecht), pp. 427-438. New York: Plenum.

Socha, J. J. (2002). Gliding flight in the paradise tree snake. *Nature* **418**, 603-604.

Socha, J. J. and LaBarbera, M. (2005). Effects of size and behavior on aerial performance of two species of flying snakes (*Chrysopelea*). *J. Exp. Biol.* **208**, 1835-1847.

Socha, J. J., O'Dempsey, T. and LaBarbera, M. (2005). A 3D kinematic analysis of gliding in a flying snake, *Chrysopelea paradisi*. *J. Exp. Biol.* **208**, 1817-1833.

Stafford, B. J., Thorington, R. W. and Kawamichi, T. (2002). Gliding behavior of Japanese giant flying squirrels (*Petaurista leucogenys*). *J. Mammal.* **83**, 553-562.

Torres, G. E. and Mueller, T. J. (2001). Aerodynamics of low aspect ratio wings. In *Fixed and Flapping Wing Aerodynamics for Micro Air Vehicle Applications*. Vol. 195 (ed. T. J. Mueller), pp. 115-142. Reston, VA: AIAA.

Vandenberghe, N., Zhang, J. and Childress, S. (2004). Symmetry breaking leads to forward flapping flight. *J. Fluid Mech.* **506**, 147-155.

Vernes, K. (2001). Gliding performance of the northern flying squirrel (*Glaucomys sabrinus*) in mature mixed forest of eastern Canada. *J. Mammal.* **82**, 1026-1033.

Wilkinson, M. T., Unwin, D. M. and Ellington, C. P. (2006). High lift function of the pteroid bone and forewing of pterosaurs. *Proc. R. Soc. Lond. B Biol. Sci.* **273**, 119-126.

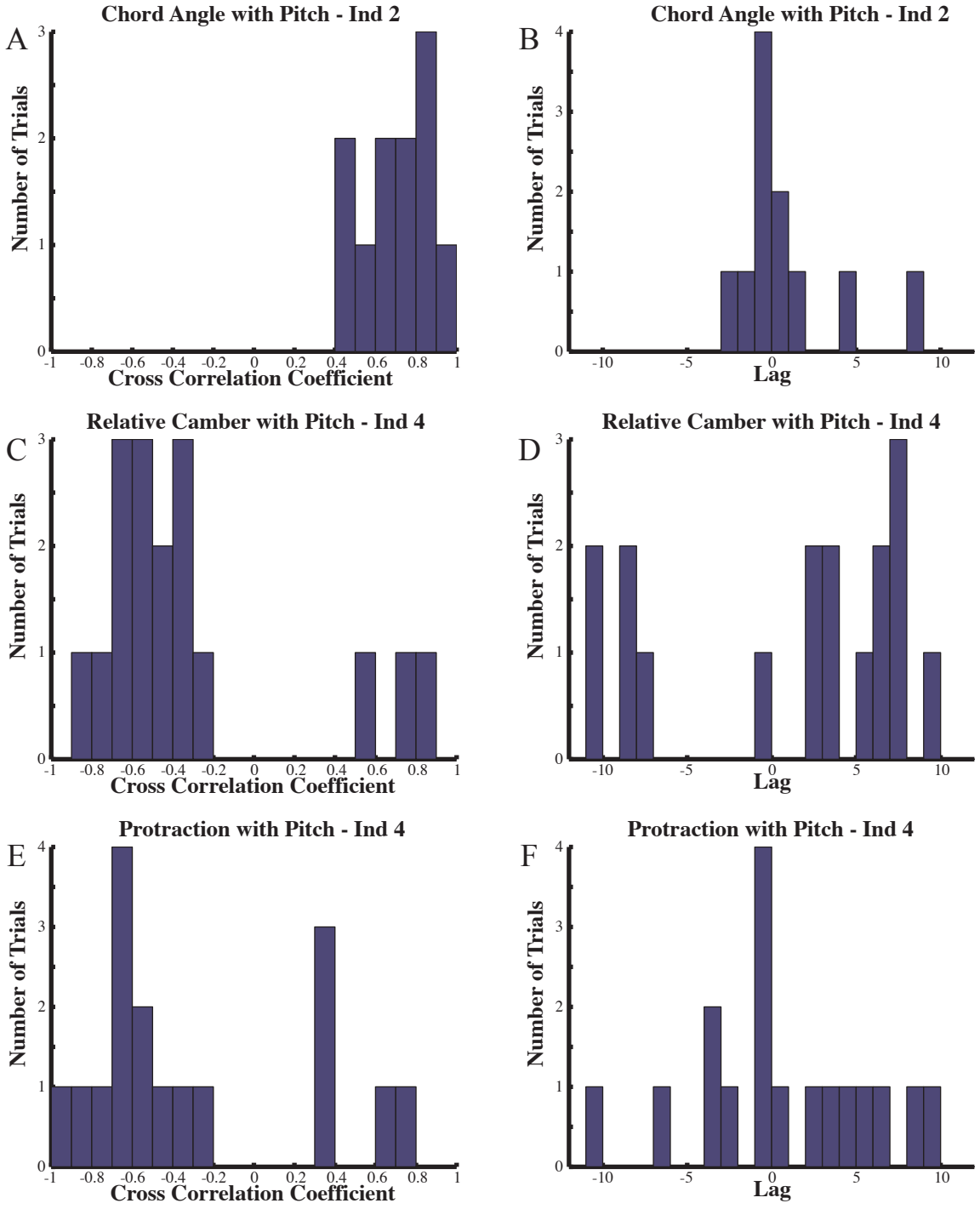
A
Chord Angle with Pitch - Ind 2
Number of Trials
Cross Correlation Coefficient
B
Chord Angle with Pitch - Ind 2
Number of Trials
Lag
C
Relative Camber with Pitch - Ind 4
Number of Trials
Cross Correlation Coefficient
D
Relative Camber with Pitch - Ind 4
Number of Trials
Lag
E
Protraction with Pitch - Ind 4
Number of Trials
Cross Correlation Coefficient
F
Protraction with Pitch - Ind 4
Number of Trials
Lag

Figure S1

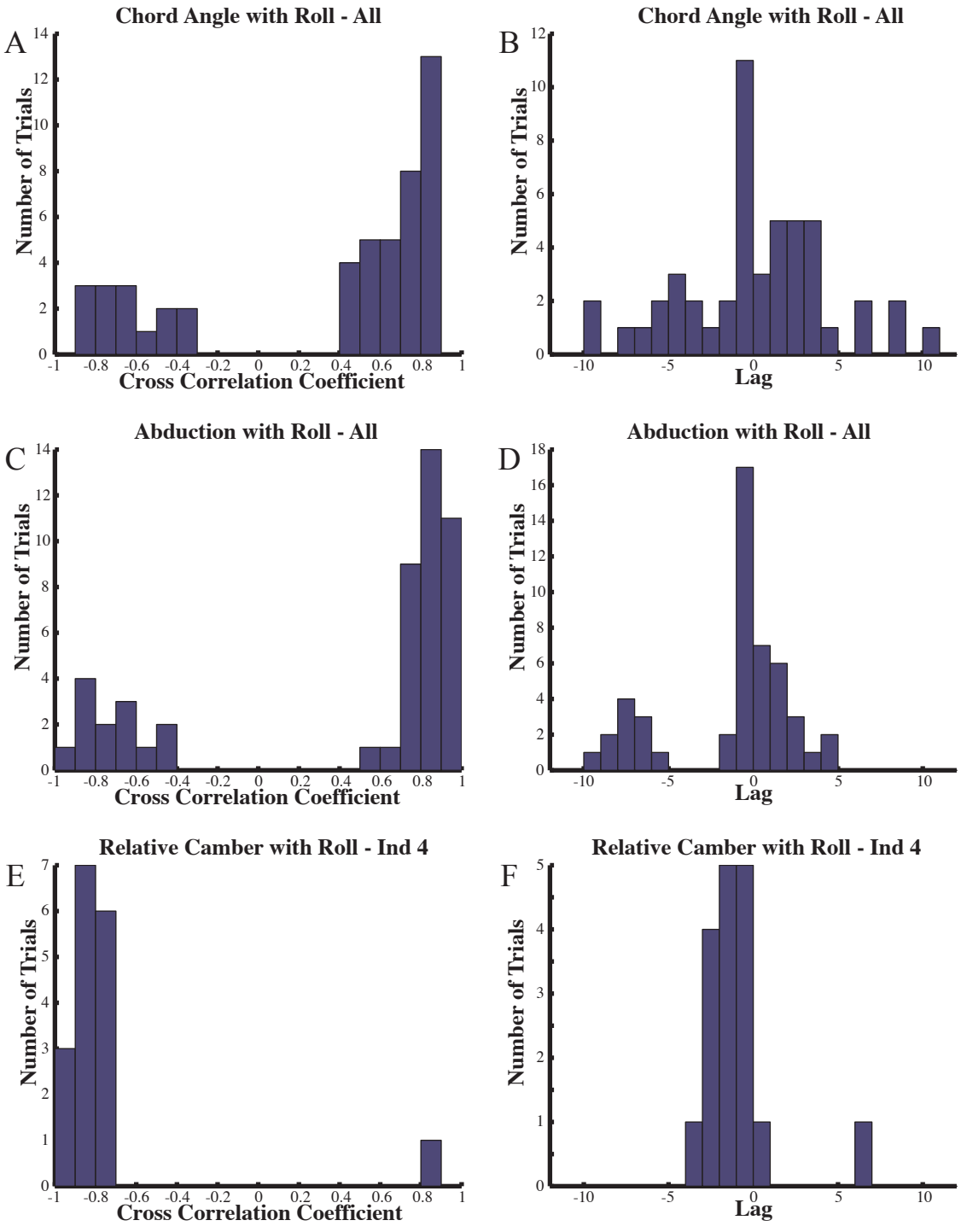
A
Chord Angle with Roll - All
Number of Trials
Cross Correlation Coefficient
B
Chord Angle with Roll - All
Number of Trials
Lag
C
Abduction with Roll - All
Number of Trials
Cross Correlation Coefficient
D
Abduction with Roll - All
Number of Trials
Lag
E
Relative Camber with Roll - Ind 4
Number of Trials
Cross Correlation Coefficient
F
Relative Camber with Roll - Ind 4
Number of Trials
Lag

Figure S2

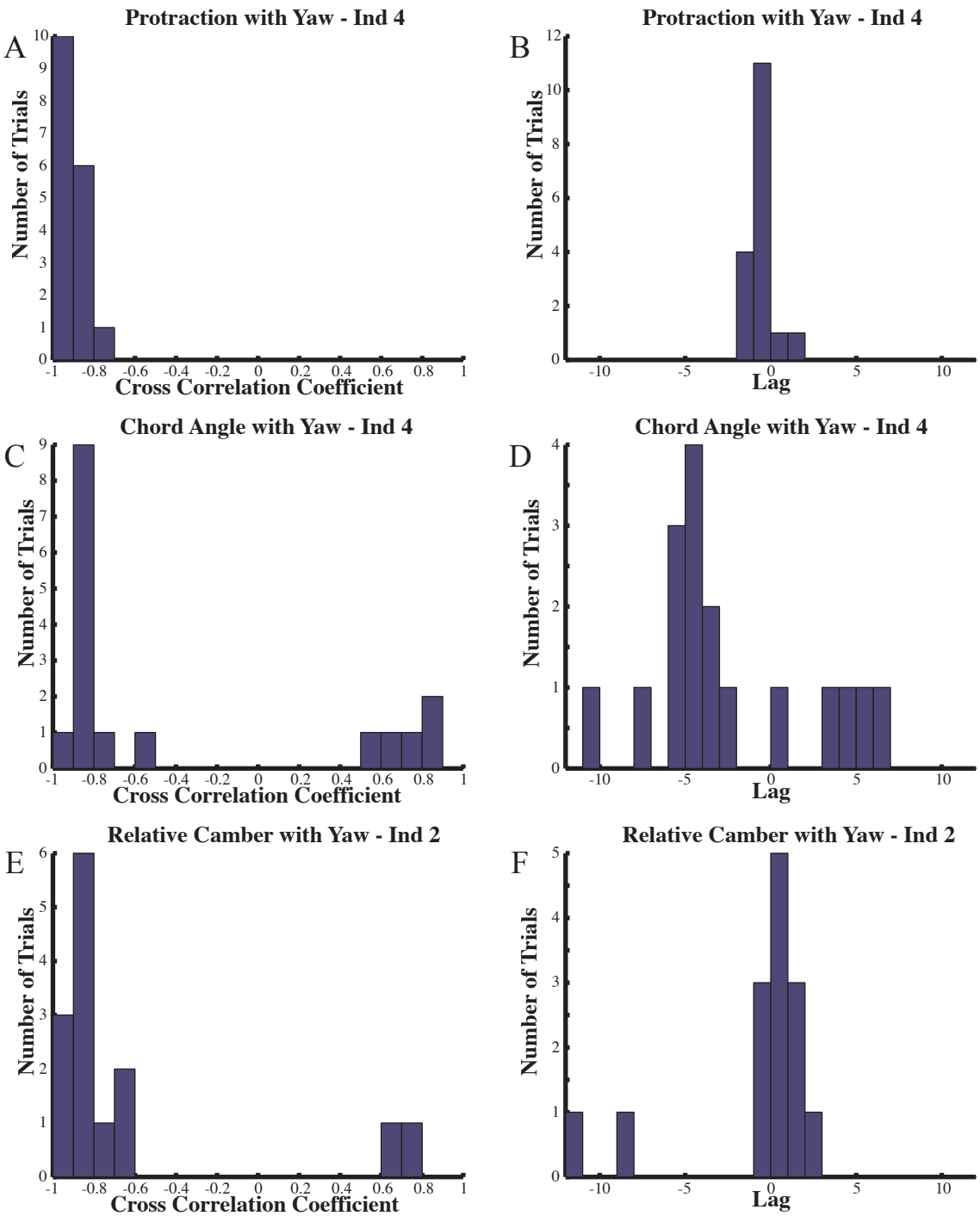
A
Protraction with Yaw - Ind 4
Number of Trials
Cross Correlation Coefficient
B
Protraction with Yaw - Ind 4
Number of Trials
Lag
C
Chord Angle with Yaw - Ind 4
Number of Trials
Cross Correlation Coefficient
D
Chord Angle with Yaw - Ind 4
Number of Trials
Lag
E
Relative Camber with Yaw - Ind 2
Number of Trials
Cross Correlation Coefficient
F
Relative Camber with Yaw - Ind 2
Number of Trials
Lag

Figure S3